Electronic supplementary information (ESI)

Synthesis of Cubane-Like Anion $[Re_4As_2S_2(CN)_{12}]^{6-}$ for Coordinate Regulation of Na^+ Ions Transport

Hongyang Li,[ab] Andrey V. Ermolaev,[b] Aleksei S. Pronin,[b] Jingang Zheng,[a] Hao Huang,[a] Han Zhang,[a] Lixiang Li,[a] Baigang An,*[a] Yuri V. Mironov*[b] and Chengguo Sun*[ac]

[a] Key Laboratory of Energy Materials and Electrochemistry Liaoning Province, School of Chemical Engineering, University of Science and Technology Liaoning, Anshan 114051, China

[b] Nikolaev Institute of Inorganic Chemistry, Siberian Branch of the Russian Academy of Sciences, Novosibirsk 630090, Russia

[c] School of Chemical Engineering, Nanjing University of Science and Technology, Nanjing, Jiangsu 210094, China

*Correspondence and requests for materials should be addressed to Yuri V. Mironov (yuri@niic.nsc.ru)

Experimental Section

1. Materials synthesis

1.1 Preparation of Cathodes and Cell Assembly

All the chemicals are commercially available and were used without purification. For raw materials polyvinylidene fluoride (PVDF), $NaVPO_4$ (NVP) and Super P (SP), they should be dried under vacuum at 60 °C for 24 h before using. The cathode electrode materials were prepared by mixing NVP (70%), SP (15%), and PVDF (15%) to be dissolved in anhydrous N-methyl-2-pyrrolidinone (NMP). The prepared slurry was cast on aluminum current collector and dried at 80 °C for 24 h in vacuum oven. The cathode foil was punched into small plates with 12 mm in diameter. Mass loading of NVP in the electrode was around 2 mg cm^{-2}. All of the cells were assembled using CR2032-type coin cells in an argon (Ar)-filled glove box ($[H_2O] < 0.1$ ppm, $[O_2] < 0.1$ ppm).

1.2 Crystallographic Data

CCDC 2329960 contain the crystallographic data for this paper. These data can be obtained free of charge from The Cambridge Crystallographic Data Centre via www.ccdc.cam.ac.uk/structures. and can be received from the authors.

2. Characterization

The scanning electron microscope (SEM, FEI Apreo S) was used to examine the surface morphology of materials. Energy dispersive X-ray (EDS, EDAX) analysis was performed with EDX detector to study the element distribution. The cross-section was obtained by cutting off the electrolyte in the glovebox.

X-ray photoelectron spectroscopy (XPS, SHIMADZU Axis Supra) analysis was conducted on the valence states of the constituent elements on Na anode surface, with Al Kα radiation. The calibration peak is C 1s at 284.8 eV. Generally, due to the water and oxygen sensitivity of Na

metal, the Na anodes for the ex situ SEM and ex situ XPS measurement were transferred by sealed cans. The cell was disassembled manually in the glove box by a nipper plier to harvest the Na anode.

The thermogravimetric analysis (TGA) and the derivative thermogravimetric (DTG) analysis of the $Na_6[Re_4As_2S_2(CN)_{12}]\cdot 0.75CH_3OH\cdot 6H_2O$ was performed using a NETZSCH TG 209 F3 carried out from 30 to 1000 °C under an N_2 flow with a heating rate of 5 °C min^{-1}.

The Fourier-transform infrared (FT-IR) analysis of the crystal water was performed using a BRUKER Alpha II carried out in the wavenumber range of 4000 to 500 cm^{-1} with 4 scans for each spectrum.

3. Density Functional Theory (DFT)

We carried out all the DFT calculations in the Vienna ab initio simulation (VASP 6.1.0) code.[1] The exchange-correlation was simulated with PBE functional, and the ion-electron interactions were described by the PAW method.[2,3] The van der Waals interactions (vdWs) interaction was included by using empirical DFT-D3 method.[4] The $Na_6[Re_4As_2S_2(CN)_{12}]$ both with and without the H_2O and CH_3OH were used to investigate the average formation energy of Na vacancy. All atoms in the structure were allowed to move freely during the geometry optimization. The Monkhorst-Pack-grid-mesh-based Brillouin zone k-points were set as 2×2×1 for all periodic structure with the cutoff energy of 450 eV. The convergence criteria were set as 0.02 eV A^{-1} and 10^{-5} eV in force and energy, respectively. The Na vacancy formation energy calculation was based on following formula:

$$\Delta E = (E_{\text{vacancy}} + E_{\text{atom}}) - E_{\text{total}}$$

Where E_{total} is the total DFT energy of the completed system, while the $E_{vacancy}$ and E_{atom} are the DFT energy of the system with Na vacancy and the DFT energy of the Na atom, respectively.

Supplementary Figures and Tables

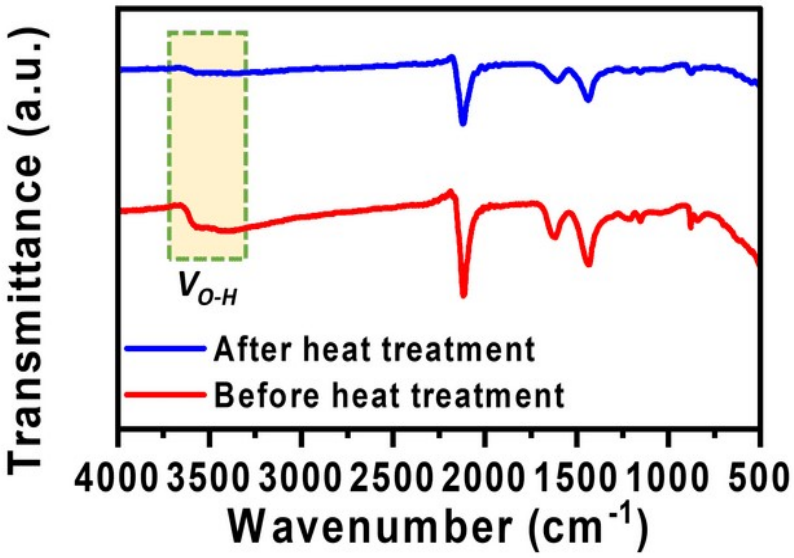

Fig. S1 FT-IR curves of $Na_6[Re_4As_2S_2(CN)_{12}]\cdot 0.75CH_3OH\cdot 6H_2O$ before and after heat treatment.

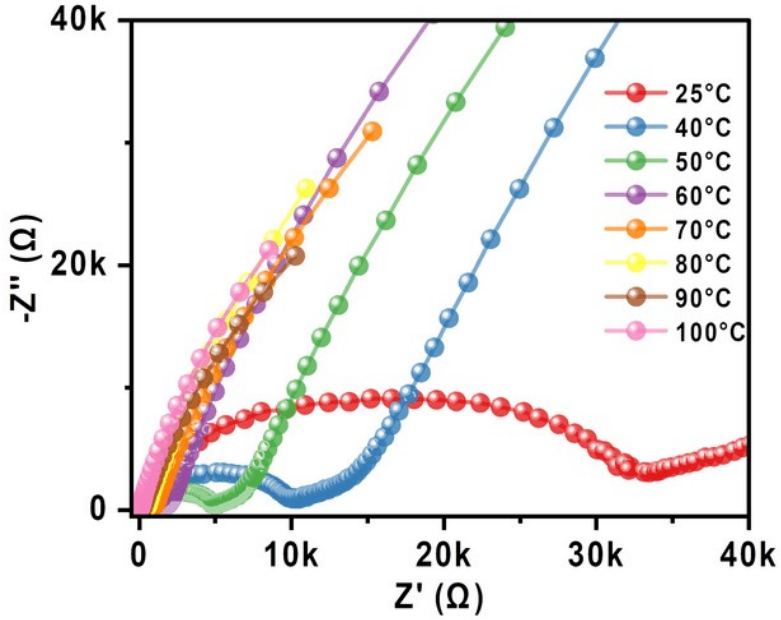

Fig. S2 The Nyquist plots of the $Na_6[Re_4As_2S_2(CN)_{12}]$ pallet at various temperature.

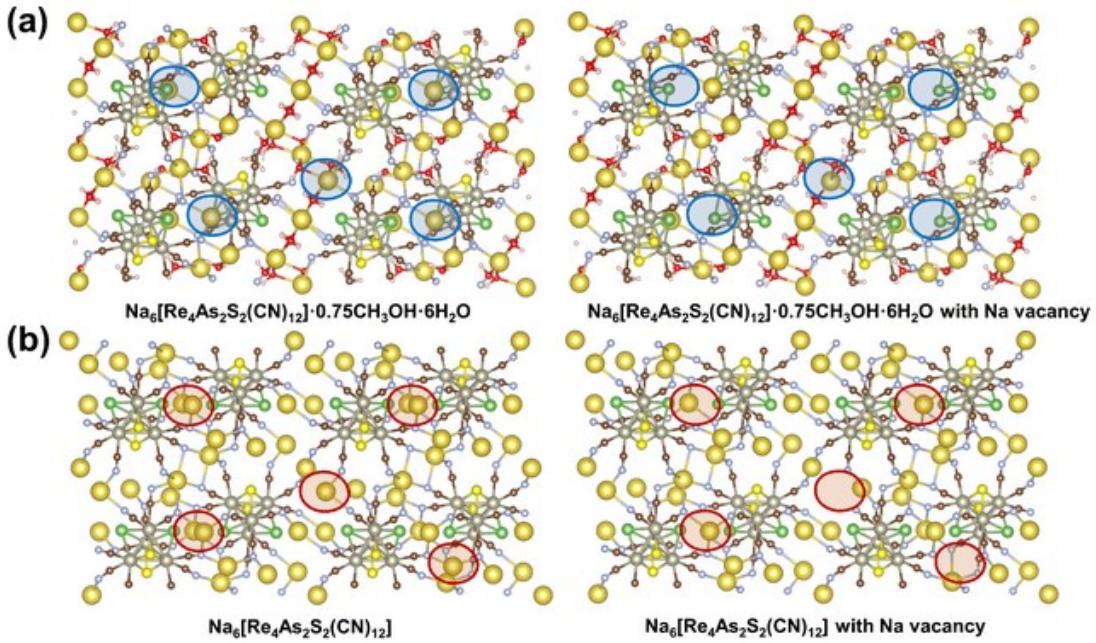

Fig. S3 Schematic diagram of crystal structure without or with Na vacancy: (a) $Na_6[Re_4As_2S_2(CN)_{12}]\cdot 0.75CH_3OH\cdot 6H_2O$, (b) $Na_6[Re_4As_2S_2(CN)_{12}]$.

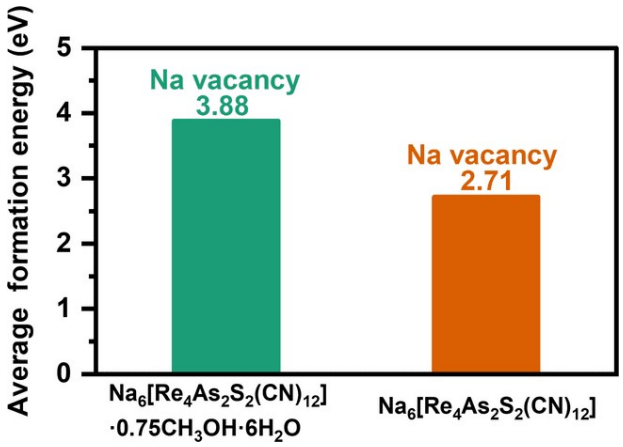

Fig. S4 Average formation energy of Na vacancy.

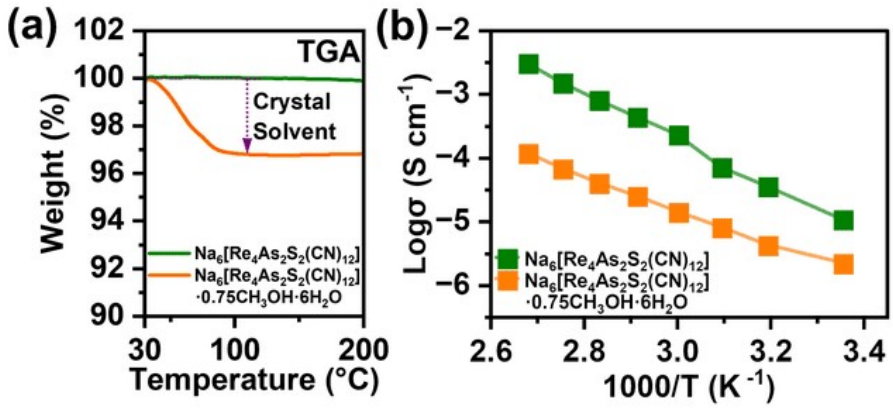

Fig. S5 (a) The TGA curves of $Na_6[Re_4As_2S_2(CN)_{12}]$ and $Na_6[Re_4As_2S_2(CN)_{12}]\cdot 0.75CH_3OH\cdot 6H_2O$. (b) The ionic conductivity curves of $Na_6[Re_4As_2S_2(CN)_{12}]$ and $Na_6[Re_4As_2S_2(CN)_{12}]\cdot 0.75CH_3OH\cdot 6H_2O$.

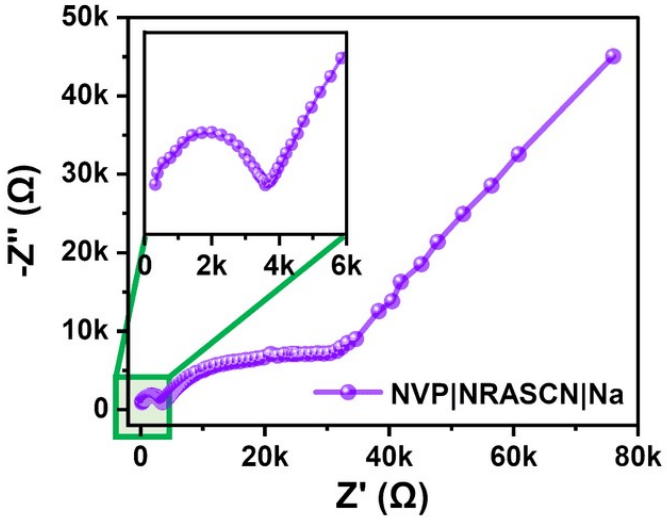

Fig. S6 Nyquist plots of the NVP | NRASCN | Na cell.

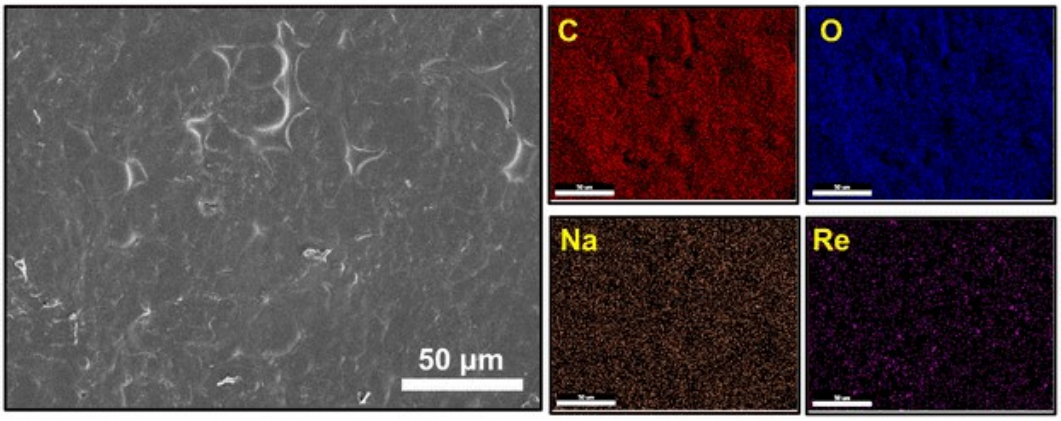

Fig. S7 SEM image of PEO-NaTFSI-NRASCN electrolyte and corresponding EDS mapping of C, O, Na and Re elements.

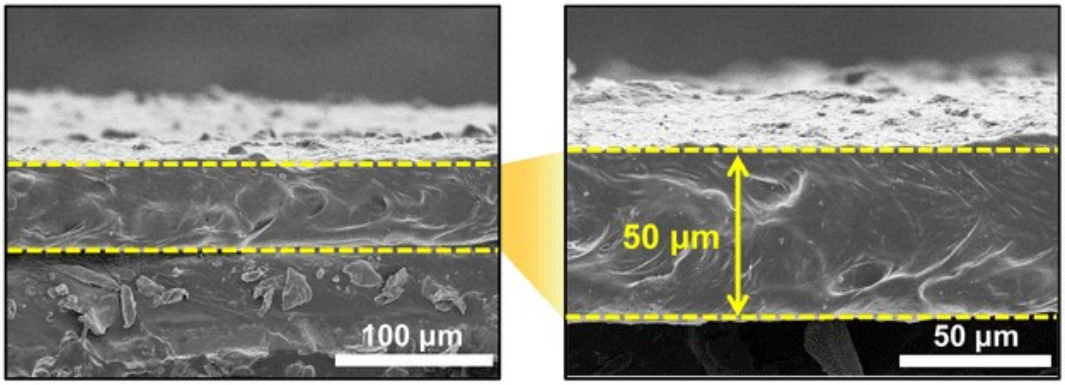

Fig. S8 Cross-sectional SEM image of PEO-NaTFSI-NRASCN electrolyte.

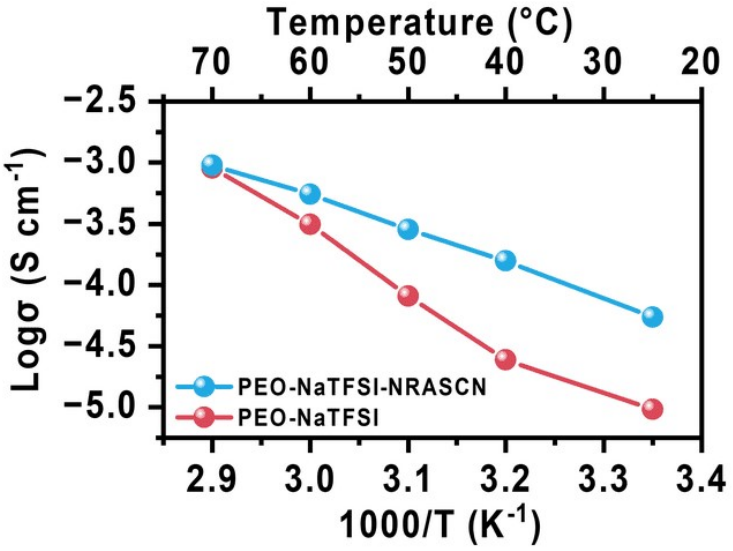

Fig. S9 Ionic conductivity of PEO-NaTFSI and PEO-NaTFSI-NRASCN electrolytes.

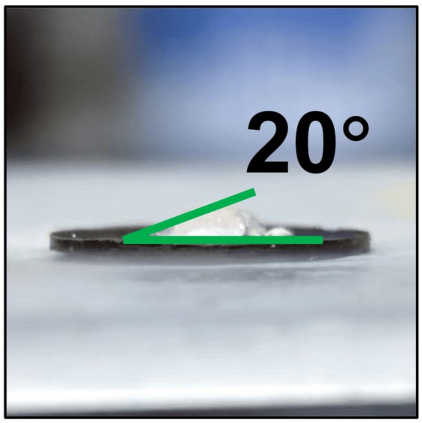

Fig. S10 Contact angle measurements of NRASCN and sodium metal.

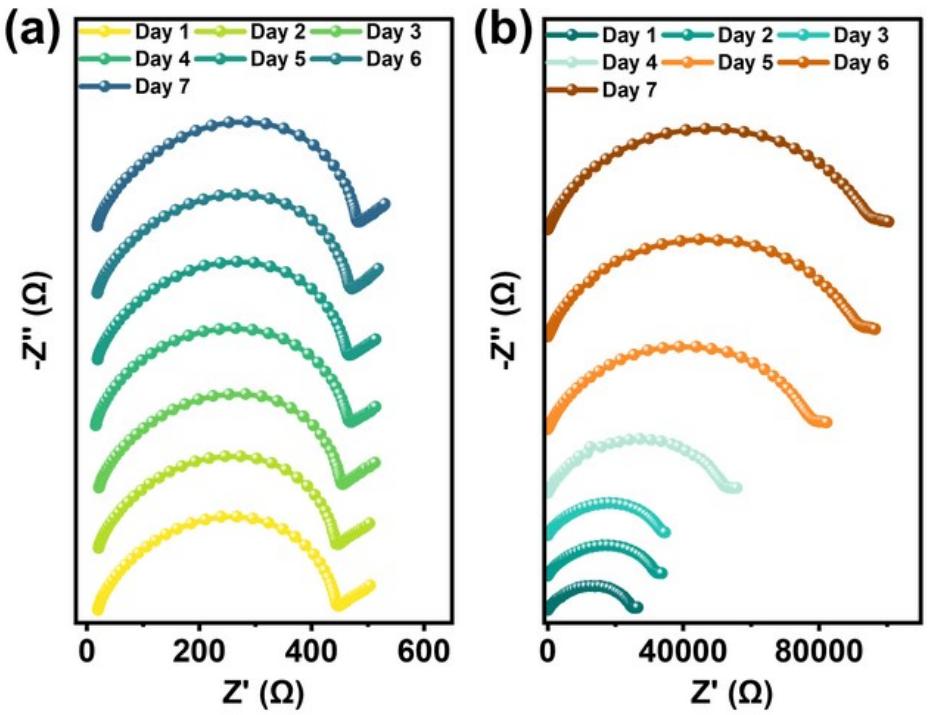

Fig. S11 (a) EIS of Na | PEO-NaTFSI-NRASCN | Na cell for different storage time. (b) EIS of Na | PEO-NaTFSI | Na cell for different storage time.

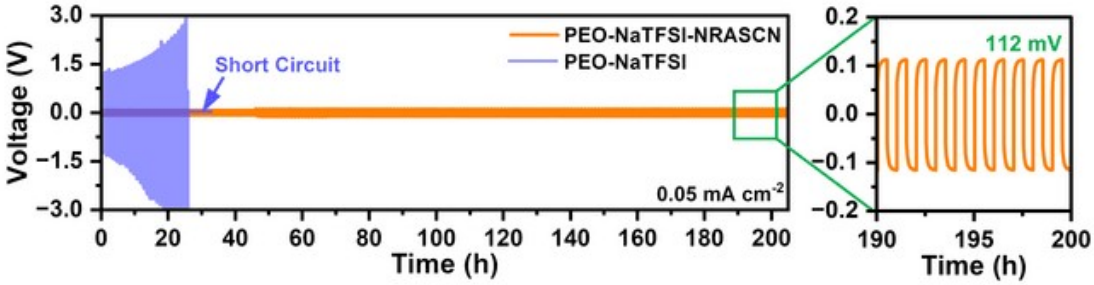

Fig. S12 Galvanostatic cycling of Na | PEO-NaTFSI-NRASCN | Na and Na | PEO-NaTFSI | Na symmetric cells of 0.05 mA cm^{-2} at 60 °C.

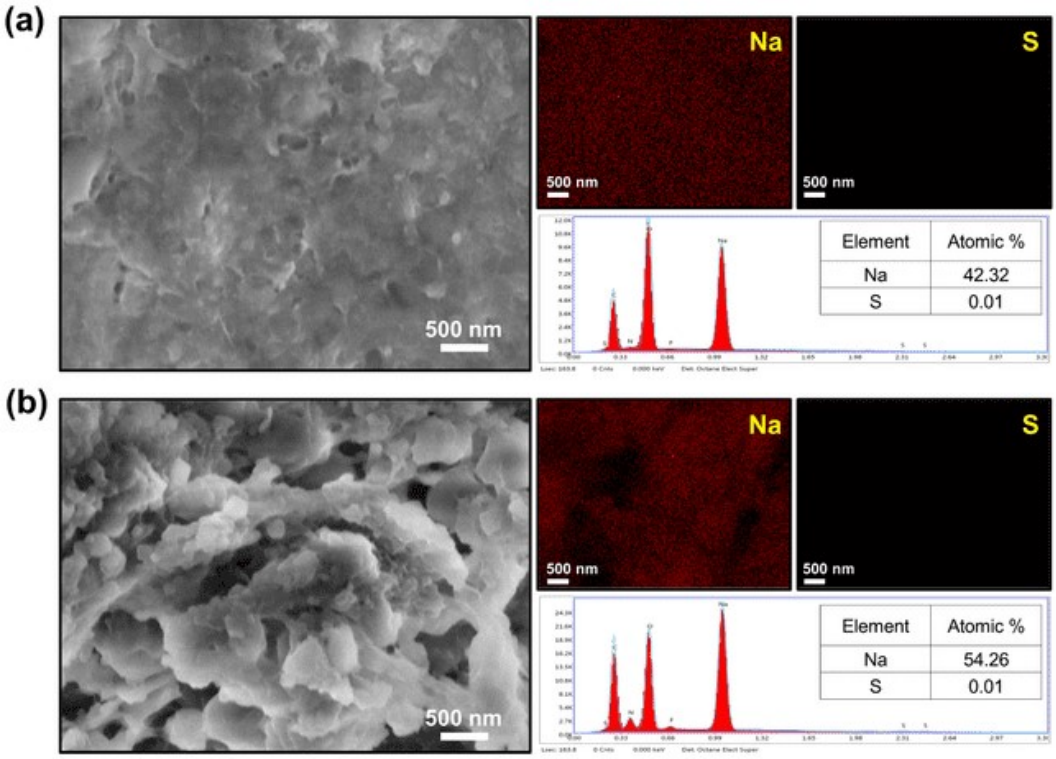

Fig. S13 SEM images of Na anode surface after 200 cycles at 0.3 C and corresponding EDS mapping, spectrum of Na, S elements: (a) PEO-NaTFSI-NRASCN, (b) PEO-NaTFSI.

Table S1 Main crystallographic data and structure refinement details for $Na_6[Re_4As_2S_2(CN)_{12}]\cdot 0.75CH_3OH\cdot 6H_2O$

	$Na_6[Re_4As_2S_2(CN)_{12}]\cdot 0.75CH_3OH\cdot 6H_2O$
Empirical formula	$C_{12.75}H_{2.25}As_{1.94}N_{12}Na_6O_{6.75}Re_4S_{2.06}$
Formula weight	1525.64
Crystal size (mm)	0.04 × 0.02 × 0.01
Crystal system	Triclinic
Space group	*P*1
a (Å)	9.4363(3)
b (Å)	10.2986(2)
c (Å)	17.6142(4)
α (°)	93.922(1)
β (°)	98.585(1)
γ (°)	104.090(1)
V (Å^3)	1631.84(7)
Z	2
ρ_{calc} (g cm^{-3})	3.105
μ(Mo-Kα), mm^{-1}	17.004
θ range (°)	2.95–27.43
R_{int}	0.0454
Reflections collected	19758
Independent reflections	7443
Observed reflections [$I > 2\sigma(I)$]	6210
Parameters refined	423
$R_1[F^2 > 2\sigma(F^2)]$	0.0321
$wR_2(F^2)$	0.0574
Goodness-of-fit on F^2	1.049
$\Delta\rho_{max}$, $\Delta\rho_{min}$ (e Å^{-3})	2.224; –1.211

Table S2 Comparison of Na^+ ion conductivity and activation energy for NRASCN with other solid-state electrolytes.

Composition	**Sintering temperature** T (°C)	**Na^+ ion conductivity** σ (S cm^{-1})	**Activation energy** Ea (eV)	**Report**
NRASCN	550	1.05×10^{-5} at r. t.	0.32	This work
$Na_{3.8}Sc_2Si_{0.8}P_{2.2}O_{12}$	1300	4×10^{-6} at r. t.	0.47	[5]
$Na_2Mg_2TeO_6$	700	2.3×10^{-4} at r. t.	0.34	[6]
0.3 Ni-NZSP	900	1.13×10^{-4} at r. t.	0.37	[7]
Na_3InCl_6	800	2.3×10^{-8} at r. t.	0.81	[8]
$NaAlCl_4$	900	3.9×10^{-6} at 30 °C	0.42	[9]
NRASCN	550	3.03×10^{-3} at 100 °C	0.32	This work
$NaBH_4@Na_2B_{12}H_{12}$	150	4×10^{-4} at 115 °C	0.57	[10]
$Na_3OBr_{0.6}I_{0.4}$	350	9.80×10^{-5} at 160 °C	0.62	[11]

Table S3 Comparison of the performance of Na-ASSBs by different PEO-based solid electrolytes and NVP cathode.

Composition	**Rate and temperature**	**Initial discharge capacity** (mAh g^{-1})	**Cycle number**	**Capacity retention**	**Report**
PEO-NaTFSI-NRASCN	0.3 C at 60 °C	109.4	1000	91.8 %	This work
PEGDA-$NaClO_4$	0.3 C at 60 °C	105	1100	91.4 %	[12]
NGFOC-G	0.5 C at 60 °C	114	150	77.1 %	[13]
NZP-PEO@IL	0.5 C at 60 °C	104.5	150	90.0 %	[14]
(10PEO-85NZSP-5PEG)-40$NaClO_4$	0.5 C at 55 °C	68.2	100	97.6 %	[15]
PEO-P-N	1 C at 60 °C	102	500	87.3 %	[16]
CEt5	0.1 C at 60 °C	112	50	46.4 %	[17]

Reference

1. G. Kresse and J. Furthmuller, Efficient iterative schemes for *ab initio* total-energy calculations using a plane-wave basis set, *Phys. Rev. B*, 1996, **54**, 11169.
2. J. P. Perdew, K. Burke and M. Ernzerhof, Generalized gradient approximation made simple, *Phys. Rev. Lett.*, 1996, **77**, 3865.
3. B. Hammer, L. B. Hansen and J. K. Norskov, Improved adsorption energetics within density-functional theory using revised perdew-burke-ernzerhof functionals, *Phys. Rev. B*, 1999, **59**, 7413.
4. S. Grimme, Semiempirical GGA-type density functional constructed with a long-range dispersion correction, *J. Comput. Chem.*, 2006, **27**, 1787-1799.
5. B. Santhoshkumar, P. L. Rao, K. V. Ramanathan, A. K. Bera, S. M. Yusuf, V. R. Hathwar and B. Pahari, Structure and ionic conductivity of $Na_{3+x}Sc_2Si_xP_{3-x}O_{12}$ (X=0.0, 0.2, 0.4, 0.8) NASICON materials: A combined neutron diffraction, MAS NMR and impedance study, *Solid State Sci.*, 2021, **111**, 106470.
6. Y. Li, Z. Deng, J. Peng, J. Gu, E. Chen, Y. Yu, J. Wu, X. Li, J. Luo, Y. Huang, Y. Xu, Z. Gao, C. Fang, J. Zhu, Q. Li, J. Han and Y. Huang, New p2-type honeycomb-layered sodium-ion conductor: $Na_2Mg_2TeO_6$, *ACS Appl. Mater. Inter.*, 2018, **10**, 15760-15766.
7. J. Luo, G. Zhao, W. Qiang and B. Huang, Synthesis of Na ion-electron mixed conductor $Na_3Zr_2Si_2PO_{12}$ by doping with transition metal elements (Co, Fe, Ni), *J. Am. Ceram. Soc.*, 2022, **105**, 3428-3437.
8. T. Zhao, A. N. Sobolev, R. Schlem, B. Helm, M. A. Kraft and W. G. Zeier, Synthesis-controlled cation solubility in solid sodium ion conductors $Na_{2+x}Zr_{1-x}In_xCl_6$, *ACS Appl. Energy Mater.*, 2023, **6**, 4334-4341.
9. J. Park, J. P. Son, W. Ko, J.-S. Kim, Y. Choi, H. Kim, H. Kwak, D.-H. Seo, J. Kim and Y. S. Jung, $NaAlCl_4$: New halide solid electrolyte for 3 V stable cost-effective all-solid-state Na-ion batteries, *ACS Energy Lett.*, 2022, **7**, 3293-3301.
10. X. Luo, A. Rawal, M. S. Salman and K.-F. Aguey-Zinsou, Core–shell $NaBH_4$@$Na_2B_{12}H_{12}$ nanoparticles as fast ionic conductors for sodium-ion batteries, *ACS Appl. Nano Mater.*, 2022, **5**, 373-379.
11. Y. Wang, Q. Wang, Z. Liu, Z. Zhou, S. Li, J. Zhu, R. Zou, Y. Wang, J. Lin and Y. Zhao, Structural manipulation approaches towards enhanced sodium ionic conductivity in Na-rich antiperovskites, *J. Power Sources*, 2015, **293**, 735-740.
12. C. Luo, Q. Li, D. Shen, R. Zheng, D. Huang and Y. Chen, Enhanced interfacial kinetics and fast Na^+ conduction of hybrid solid polymer electrolytes for all-solid-state batteries, *Energy Stor. Mater.*, 2021, **43**, 463-470.
13. Q. Yu, J. Hu, X. Nie, Y. Zeng and C. Li, Liquid metal mediated heterostructure fluoride solid electrolytes of high conductivity and air stability for sustainable Na metal batteries, *ACS Nano*, 2024, **18**, 5790-5804.
14. L. Shen, S. Deng, R. Jiang, G. Liu, J. Yang and X. Yao, Flexible composite solid electrolyte with 80 wt% $Na_{3.4}Zr_{1.9}Zn_{0.1}Si_{2.2}P_{0.8}O_{12}$ for solid-state sodium batteries, *Energy Stor. Mater.*, 2022, **46**, 175-181.
15. W. Niu, L. Chen, Y. Liu and L.-Z. Fan, All-solid-state sodium batteries enabled by flexible composite electrolytes and plastic-crystal interphase, *Chem. Eng. J.*, 2020, **384**, 123233.
16. E. Matios, H. Wang, J. Luo, Y. Zhang, C. Wang, X. Lu, X. Hu, Y. Xu and W. Li, Reactivity-guided formulation of composite solid polymer electrolytes for superior sodium metal batteries, *J. Mater. Chem. A*, 2021, **9**, 18632-18643.
17. W. Yu, Y. Zhai, G. Yang, J. Yao, S. Song, S. Li, W. Tang, N. Hu and L. Lu, A composite electrolyte with $Na_3Zr_2Si_2PO_{12}$ microtube for solid-state sodium-metal batteries, *Ceram. Int.*, 2021, **47**, 11156-11168.